

A New Quadruply Lensed Quasar: SDSS J125107.57+293540.5

Issha Kayo¹, Naohisa Inada^{2,3}, Masamune Oguri^{4,5}, Patrick B. Hall⁶, Christopher S. Kochanek⁷, Gordon T. Richards^{8,9}, Donald P. Schneider¹⁰, Donald G. York¹¹, and Kaike Pan¹²

ABSTRACT

We report the discovery of a quadruply imaged quasar, SDSS J125107.57+293540.5, selected from the Sloan Digital Sky Survey. Follow-up imaging reveals that the system consists of four blue point-like components in a typical cusp lens geometry surrounding a central red galaxy. The source redshift is 0.802 and the lens redshift is 0.410. The maximum image separation between the lensed components is $1''.79$. While the image configuration is well reproduced by standard mass models with reasonable parameter values, the flux ratios predicted by these models differ from the

¹Department of Physics and Astrophysics, Nagoya University, Chikusa-ku, Nagoya 464-8602, Japan.

²Institute of Astronomy, Faculty of Science, University of Tokyo, 2-21-1 Osawa, Mitaka, Tokyo 181-0015, Japan.

³Cosmic Radiation Laboratory, RIKEN (The Physical and Chemical Research Organization), 2-1 Hiro-sawa, Wako, Saitama 351-0198, Japan.

⁴Kavli Institute for Particle Astrophysics and Cosmology, Stanford University, 2575 Sand Hill Road, Menlo Park, CA 94025, USA

⁵Princeton University Observatory, Peyton Hall, Princeton, NJ 08544, USA

⁶Department of Physics and Astronomy, York University, 4700 Keele Street, Toronto, Ontario, M3J 1P3, Canada

⁷Department of Astronomy, The Ohio State University, 4055 McPherson Lab, 140 West 18th Avenue, Columbus, OH 43210, USA

⁸Johns Hopkins University, 3400 N. Charles St., Baltimore, MD 21218, USA

⁹Department of Physics, Drexel University, 3141 Chestnut Street, Philadelphia, PA 19104, USA

¹⁰Department of Astronomy and Astrophysics, The Pennsylvania State University, University Park, PA 16802, USA

¹¹Department of Astronomy and Astrophysics, University of Chicago, Enrico Fermi Institute, 5640 South Ellis Avenue, Chicago, IL 60637, USA

¹²Apache Point Observatory, New Mexico State Univ., P. O. Box 59, Sunspot, NM 88349, USA

observed ratios in all bands. This is suggestive of small-scale structures in this lens, although the definitive identification of the anomaly requires more accurate photometry and astrometry.

Subject headings: gravitational lensing — quasars: individual (SDSS J125107.57+293540.5)

1. Introduction

Nearly one hundred gravitationally lensed quasars have been found to date (see the review by Kochanek 2006), and they have become a unique astronomical and cosmological tool. Their usefulness is particularly enhanced by constructing a statistical sample with a well-understood selection function with the help of extensive and homogeneous surveys such as the HST Snapshot Survey (Maoz et al. 1993) or the Cosmic Lens All Sky Survey (CLASS; Myers et al. 2003; Browne et al. 2003). However, the number of strongly lensed quasars in systematic surveys is still limited. To construct a larger lens sample, we are conducting the SDSS Quasar Lens Search (SQLS; Oguri et al. 2006) based on spectroscopic quasar catalogs (Schneider et al. 2005, 2007) produced by the Sloan Digital Sky Survey (SDSS; York et al. 2000). Thus far, it has discovered 16 galaxy-scale and 2 cluster-scale lensed quasars (Inada et al. 2003a,b, 2005, 2006a,b, 2007; Johnston et al. 2003; Morgan et al. 2003; Pindor et al. 2004, 2006; Oguri et al. 2004, 2005; Morokuma et al. 2007) and re-discovered 8 previously known lensed quasars (Walsh et al. 1979; Weymann et al. 1980; Surdej et al. 1987; Magain et al. 1988; Bade et al. 1997; Oscoz et al. 1997; Schechter et al. 1998; Morgan et al. 2001). A significant fraction of our lens candidates still require follow-up observations, so we expect to discover more lensed quasars in the coming years.

In this paper, we report the discovery of a quadruply lensed quasar, SDSS J125107.57+293540.5 (SDSS J1251+2935), in the course of the SQLS. Quadruple lenses, which constitute roughly one-third of all lensed quasars, are not only visually interesting objects due to their characteristic morphologies but also scientifically important and useful objects. Four image lenses provide many more constraints on the mass distribution of the lens. In particular, the image flux ratios expected for smooth, central potentials are relatively well-defined and the differences between the observed and model flux ratios can be used to study gravitational substructures (e.g., Mao & Schneider 1998). Anomalous flux ratios, where the observed and model image fluxes are in significant disagreement are fairly common and are due to the combined effects of the stars in the lens galaxy and satellite halos. In radio lenses this has been used to argue that the abundance of satellite halos is consistent with the predictions of standard CDM models (e.g., Metcalf & Madau 2001; Chiba 2002; Kochanek & Dalal 2004), while in optical lenses the effects of substructure and microlensing by the stars must be

disentangled (e.g., Chiba et al. 2005; Keeton et al. 2006; Morgan et al. 2006).

In the next section, we briefly describe our algorithm for candidate selection from the SDSS data. Details of follow-up imaging using the University of Hawaii 2.2-meter (UH88) telescope are provided in § 3. We investigate mass models of the system in § 4, and summarize our results in § 5. Throughout the paper we assume a cosmological model with matter density $\Omega_M = 0.27$, cosmological constant $\Omega_\Lambda = 0.73$, and Hubble constant $h = H_0/(100\text{km s}^{-1}\text{Mpc}^{-1}) = 0.7$ (Spergel et al. 2003).

2. SDSS Data

The SDSS is conducting both a photometric survey (Gunn et al. 1998; Lupton et al. 1999; Stoughton et al. 2002; Tucker et al. 2006) in five broad-band optical filters (Fukugita et al. 1996) and a spectroscopic survey with a multi-fiber spectrograph covering 3800 Å to 9200 Å at a resolution of $R \sim 1850$. The SDSS uses a dedicated wide-field (3° field of view) 2.5-m telescope (Gunn et al. 2006) at the Apache Point Observatory in New Mexico, USA, covering 10,000 square degrees of the sky approximately centered on the North Galactic Cap. The imaging data are processed by the photometric pipeline (Lupton et al. 2001), and spectroscopic quasar targets are selected from the imaging data according to the algorithm described by Richards et al. (2002). Fibers for the spectroscopic observations are assigned according to the tiling algorithm of Blanton et al. (2003). The imaging data have an astrometric accuracy better than about $0''.1$ rms per coordinate (Pier et al. 2003) and photometric zeropoint errors less than about 0.03 magnitude over the entire survey area (Hogg et al. 2001; Smith et al. 2002; Ivezić et al. 2004). SDSS J1251+2935 is contained in Data Release 5 (for the imaging data; Adelman-McCarthy 2007) and later (for the spectroscopic data).

SDSS J1251+2935 was selected as a lensed quasar candidate using the morphological selection algorithm described in Oguri et al. (2006). The algorithm uses the SDSS morphological classification parameter `objc_type` and likelihood `star_L` that an object is fitted by a point-spread function (PSF). Although lensed quasar systems with small image separations are classified as single objects in the SDSS data, the profiles are extended and are not consistent with either PSF profiles or simple galaxy profiles. Therefore, small separation lensed quasar candidates are selected as objects that have very small values of `star_L`. In addition, SDSS J1251+2935 satisfies additional selection requirements based on fits to the image with GALFIT (Peng et al. 2002) which are applied to exclude false positives by single quasars. While some single quasars can pass the initial selection step, fits to such systems using two PSFs lead to either very large magnitude differences or very small image separations that are indicative of systematic errors rather than a gravitational lens (see § 5 of Oguri et al.

(2006)).

The SDSS *i*-band image of SDSS J1251+2935 is shown in Figure 1. The PSF magnitudes of SDSS J1251+2935 (after correcting for Galactic extinction) are 19.83 ± 0.04 , 19.38 ± 0.02 , 19.13 ± 0.03 , 18.85 ± 0.03 , and 18.42 ± 0.04 in *u*, *g*, *r*, *i*, and *z*, respectively. SDSS J1251+2935 is spectroscopically confirmed as a quasar at $z = 0.802$ (see Figure 2 for the SDSS spectrum). In this spectrum, we can also see a series of absorption lines that indicate the presence of a bright early-type galaxy at $z = 0.410 \pm 0.001$. The presence of both components is a strong indication that this system is a gravitational lens.

3. Imaging Follow-up Observations

Deeper and higher-resolution optical images of SDSS J1251+2935 were obtained on 2006 April 25 (0".8 seeing) and 2006 May 3 (1".0 seeing) using the 8k mosaic CCD camera (UH8k, pixel scale of 0".232 pixel⁻¹) and the Orthogonal Parallel Transfer Imaging Camera (Optic, pixel scale of 0".137 pixel⁻¹) at the UH88 telescope, respectively. We took *V*- and *I*-band images (270 sec exposure for each band) with the UH8k, and *B*-, *R*-, and *I*-band images (400 sec exposure for each band) with the Optic. Because the night of UH8k imaging was not photometric, we did not photometrically calibrate the UH8k images. We binned (2×2) the Optic images and used them for the astrometry and photometry of the system. The 2×2 binned Optic images (*BRI*) and the original UH8k image (*V*) are shown in the left panel of Figure 3 and the upper panels of Figure 4.

We used GALFIT to model these images with a series of models of increasing complexity. The only model that works well consists of 4 point sources and a central galaxy modeled with a Sérsic profile. In Figure 3, we demonstrate that subtracting 4 fitted PSFs from the Optic *I*-band image leaves an extended object or vice versa. If we further subtract the galaxy component, there remains virtually no residual. The lower panels of Figure 4 summarize the residuals after subtracting the best models for each band's image. The galaxy flux is well-determined only in the *R* and *I*-band images, so we neglected this component in the *B* and *V*-band fits even though there are hints of its presence in the *V*-band residuals. We label the 4 point sources A–D in order of increasing *I*-band magnitudes and the central galaxy as G. We estimated that the galaxy has an effective radius of $1''.11 \pm 0''.38$, ellipticity of 0.28 ± 0.09 , the Sérsic index of 2.4 ± 1.1 , and a major axis position angle of $26^\circ \pm 5^\circ$. The *R*–*I* color of G, 0.89 ± 0.30 , is consistent with an early-type galaxy at the measured redshift (Fukugita et al. 1995). Table 1 summarizes the relative astrometry and photometry of the system, where we defined the errors from the scatter between the fits using 6 different PSF templates rather than the smaller statistical uncertainties of the individual fits. The errors are an order of

magnitude larger than other systems where images are resolved even by visual inspection. We plot the color-color diagram ($B-R$ and $R-I$) of the 4 point-like components in Figure 5 and the flux ratios between the point-like components in Figure 6. Although the colors (and flux ratios) of the lensed images have large scatter among the images, they are consistent with each other given the large uncertainties.

In Figure 1, we also labeled the nearby galaxies by their $R-I$ colors as measured using SExtractor (Bertin & Arnouts 1996). There are several galaxies with colors similar to the lens galaxy to the Southwest ($1.0 < R-I < 1.1$), and a larger group of generally bluer galaxies ($0.6 < R-I < 1.0$) $\sim 40''$ to the North. This suggests that the lens is associated with a group, as is quite common among lensed quasars (e.g., Fassnacht & Lubin 2002; Oguri et al. 2005; Oguri 2006; Williams et al. 2006).

4. Mass Modeling

We modeled the system using the *lensmodel* package (Keeton 2001) to determine whether reasonable mass distributions can reproduce the observations. We first used the 7 parameter singular isothermal ellipsoid model (SIE; the Einstein radius R_E , the ellipticity e and its position angle θ_e , and the positions of the galaxy and the source quasar) to fit the relative positions of the A–D and G components measured from the R -band image. The model fits the data well with $\chi_{\text{red}}^2 \equiv \chi^2/\text{dof} = 1.1$ for $\text{dof} = 3$ degrees of freedom. The model parameters are presented in Table 2 and the fit is illustrated in Figure 7. The predicted position angle of the lens galaxy, 19° , is reasonably consistent with the measured position angle of $26^\circ \pm 5^\circ$, which is typical for gravitational lenses (Keeton et al. 1998; Koopmans et al. 2006). Based on the Einstein radius of the model, the Faber-Jackson relations for gravitational lenses measured by Rusin et al. (2003) predict a lens galaxy apparent magnitude of $R = 19.24$ ($I = 18.57$) that agrees well with the measurement of $R = 19.32 \pm 0.16$ ($I = 18.43 \pm 0.25$).

Good fits to quadruple lenses generally require both the ellipticity of the lens and an external shear (Keeton et al. 1997), so for our second model we added a shear to the SIE model (the shear amplitude γ and its position angle θ_γ). In this case, the best fit model overfits the data ($\chi_{\text{red}}^2 = 0.062$ for $\text{dof} = 1$). Although the resulting large amplitude of the external shear is not inconsistent with N-body simulations (e.g., Holder & Schechter 2003), the lens galaxy position angle is misaligned with respect to the observations. Moreover, the large ellipticity and external shear cross almost perpendicularly, which indicates that the model may not be realistic. If we add weak constraints to match the axis ratio and position angle of the SIE component to the visible galaxy ($e = 0.28 \pm 0.15$ and $\theta_e = 26^\circ \pm 10^\circ$), then we obtain a good fit ($\chi_{\text{red}}^2 = 1.2$ for $\text{dof}=3$) with a small external shear ($\gamma = 0.02$).

This suggests that external shear is not important for fitting the image positions despite the possible existence of nearby groups.

In all these models, the predicted flux ratios differ from the observed flux ratios (see Table 2 and Figure 6). This remains the case if we add the flux ratios and their measurement errors as model constraints. The cusp relation (see Keeton et al. 2003) provides a means of determining whether the flux ratios of the three cusp images are consistent with any smooth mass distribution. In this case we find $R_{\text{cusp}} = 0.13$ and $d/R_E = 1.25$ based on the R -band flux ratios and the SIE model, which is marginally consistent with the range of distributions found for smooth lens models. The origin of the problem is presumably substructure in the gravitational potential of the lens due to either microlensing by the stars or sub-halos, since the observed flux ratios show no significant wavelength dependence. We note, however, that evidence for anomalous flux ratios is not conclusive, mainly because of large astrometric and photometric errors.

5. Summary

We report the discovery of the quadruply imaged quasar SDSS J1251+2935. The lensing hypothesis is confirmed by the facts that i) the SDSS spectrum of the system shows the emission lines of a quasar at $z_s = 0.802$ and the absorption lines of a galaxy at $z_l = 0.410$, ii) the UH8k and Optic images confirm that the system consists of 4 blue point-like components and an extended object whose color is consistent with an elliptical galaxy at $z \sim 0.4$, iii) the geometry of the system is that of a typical cusp lens and can be well reproduced by a SIE model with reasonable parameter values, and iv) the luminosity of the lens galaxy is consistent with the expected luminosity from the Faber-Jackson relation. This system is the second lowest redshift lensed quasar after RXJ1131-1231 (Sluse et al. 2003) at $z_s = 0.66$. The flux ratios of the three cusp images of the lens show a modest flux ratio anomaly, whose origins could be better constrained with higher resolution images under better observing conditions.

We thank Atsunori Yonehara for many useful comments and the anonymous referee for suggestions to improve the manuscript. Use of the UH 2.2-m telescope for the observations is supported by NAOJ. I. K. acknowledges the support from Ministry of Education, Culture, Sports, Science, and Technology, Grant-in-Aid for Encouragement of Young Scientists (No. 17740139). N. I. acknowledges supports from the Japan Society for the Promotion of Science and the Special Postdoctoral Researcher Program of RIKEN. This work was supported in part by Department of Energy contract DE-AC02-76SF00515.

Funding for the creation and distribution of the SDSS Archive has been provided by the Alfred P. Sloan Foundation, the Participating Institutions, the National Aeronautics and Space Administration, the National Science Foundation, the U.S. Department of Energy, the Japanese Monbukagakusho, and the Max Planck Society. The SDSS Web site is <http://www.sdss.org/>.

The SDSS is managed by the Astrophysical Research Consortium for the Participating Institutions. The Participating Institutions are the American Museum of Natural History, Astrophysical Institute Potsdam, University of Basel, Cambridge University, Case Western Reserve University, University of Chicago, Drexel University, Fermilab, the Institute for Advanced Study, the Japan Participation Group, Johns Hopkins University, the Joint Institute for Nuclear Astrophysics, the Kavli Institute for Particle Astrophysics and Cosmology, the Korean Scientist Group, the Chinese Academy of Sciences (LAMOST), Los Alamos National Laboratory, the Max-Planck-Institute for Astronomy (MPIA), the Max-Planck-Institute for Astrophysics (MPA), New Mexico State University, Ohio State University, University of Pittsburgh, University of Portsmouth, Princeton University, the United States Naval Observatory, and the University of Washington.

REFERENCES

- Adelman-McCarthy, J. K., et al. 2007, ApJS, submitted
- Bade, N., Siebert, J., Lopez, S., Voges, W., & Reimers, D. 1997, A&A, 317, L13
- Bertin, E. & Arnouts, S. 1996, A&AS, 117, 393
- Blanton, M. R., Lin, H., Lupton, R. H., Maley, F. M., Young, N., Zehavi, I., & Loveday, J. 2003, AJ, 125, 2276
- Browne, I. W. A., et al. 2003, MNRAS, 341, 13
- Cardelli, J. A., Clayton, G. C., & Mathis, J. S. 1989, ApJ, 345, 245
- Chiba, M. 2002, ApJ, 565, 17
- Chiba, M., Minezaki, T., Kashikawa, N., Kataza, H., & Inoue, K. T. 2005, ApJ, 627, 53
- Fassnacht, C. D. & Lubin, L. M. 2002, AJ, 123, 627
- Fukugita, M., Ichikawa, T., Gunn, J. E., Doi, M., Shimasaku, K., & Schneider, D. P. 1996, AJ, 111, 1748

- Fukugita, M., Shimasaku, K., & Ichikawa, T. 1995, *PASP*, 107, 945
- Gunn, J. E., et al. 1998, *AJ*, 116, 3040
- Gunn, J. E., et al. 2006, *AJ*, 131, 2332
- Hogg, D. W., Finkbeiner, D. P., Schlegel, D. J., & Gunn, J. E. 2001, *AJ*, 122, 2129
- Holder, G. P., & Schechter, P. L. 2003, *ApJ*, 589, 688
- Inada, N., et al. 2007, *AJ*, 133, 206
- Inada, N., et al. 2006a, *AJ*, 131, 1934
- Inada, N., et al. 2006b, *ApJ*, 653, L97
- Inada, N., et al. 2005, *AJ*, 130, 1967
- Inada, N., et al. 2003a, *AJ*, 126, 666
- Inada, N., et al. 2003b, *Nature*, 426, 810
- Ivezić, Ž., et al. 2004, *AN*, 325, 583
- Johnston, D. E., et al. 2003, *AJ*, 126, 2281
- Keeton, C. R., Burles, S., Schechter, P. L., & Wambsganss, J. 2006, *ApJ*, 639, 1
- Keeton, C. R., Gaudi, B. S., & Petters, A. O. 2003, *ApJ*, 598, 138
- Keeton, C. R. 2001, preprint (astro-ph/0102340)
- Keeton, C. R., Kochanek, C. S., & Falco, E. E. 1998, *ApJ*, 509, 561
- Keeton, C. R., Kochanek, C. S., & Seljak, U. 1997, *ApJ*, 482, 604
- Kochanek, C.S., 2006, in *Gravitational Lensing: Strong Weak and Micro*, Saas-Fee Advanced Course 33, G. Meylan, P. North, P. Jetzer, eds., (Springer: Berlin) 91 (astro-ph/0407232)
- Kochanek, C. S., Dalal, N. 2004, *ApJ*, 610, 69
- Koopmans, L. V. E., Treu, T., Bolton, A. S., Burles, S., Moustakas, L. A. 2006, *ApJ*, 649, 599
- Landolt, A. U. 1992, *AJ*, 104, 340

- Lupton, R., Gunn, J. E., Ivezić, Z., Knapp, G. R., Kent, S., & Yasuda, N. 2001, in ASP Conf. Ser. 238, *Astronomical Data Analysis Software and Systems X*, ed. F. R. Harnden, Jr., F. A. Primini, and H. E. Payne (San Francisco: Astr. Soc. Pac.), p. 269 (astro-ph/0101420)
- Lupton, R. H., Gunn, J. E., & Szalay, A. S. 1999, *AJ*, 118, 1406
- Magain, P., Surdej, J., Swings, J. -P., Borgeest, U., & Kayser, R. 1988, *Nature*, 334, 325
- Maoz, D., Bahcall, J. N., Schneider, D. P., Bahcall, N. A., Djorgovski, S., Doxsey, R., Gould, A., Kirhakos, S., Meylan, G., Yanny, B. 1993, *ApJ*, 409, 28
- Mao, S., & Schneider, P. 1998, *MNRAS*, 295, 587
- Metcalf, R. B., & Madau, P. 2001, *ApJ*, 563, 9
- Morgan, C. W., Kochanek, C. S., Morgan, N. D., & Falco, E. E. 2006, *ApJ*, 647, 874
- Morgan, N. D., Snyder, J. A., & Reens, L. H. 2003, *AJ*, 126, 2145
- Morgan, N. D., Becker, R. H., Gregg, M. D., Schechter, P. L., & White, R. L. 2001, *AJ*, 121, 611
- Morokuma, et al. 2007, *AJ*, 133, 214
- Myers, S. T., et al. 2003, *MNRAS*, 341, 1
- Oguri, M., 2006, *MNRAS*, 367, 1241
- Oguri, M., et al. 2006, *AJ*, 132, 999
- Oguri, M., et al. 2005, *ApJ*, 622, 106
- Oguri, M., Keeton, C. R., Dalal, N. 2005, *MNRAS*, 364, 1451
- Oguri, M., et al. 2004, *PASJ*, 56, 399
- Oscos, A., Serra-Ricart, M., Mediavilla, E., Buitrago, J., & Goicoechea, L. J. 1997, *AJ*, 491, L7
- Peng, C. Y., Ho, L. C., Impey, C. D., & Rix, H.-W. 2002, *AJ*, 124, 266
- Pier, J. R., Munn, J. A., Hindsley, R. B., Hennessy, G. S., Kent, S. M., Lupton, R. H., & Ivezić, Ž. 2003, *AJ*, 125, 1559

- Pindor, B., et al. 2004, AJ, 127, 1318
- Pindor, B., et al. 2006, AJ, 131, 41
- Richards, G. T., et al. 2002, AJ, 123, 2945
- Rusin, D., Kochanek, C. S., Falco, E. E., Keeton, C. R., McLeod, B. A., Impey, C. D., Lehár, J., Muñoz, J. A., Peng, C. Y., & Rix H.-W. 2003, ApJ, 587, 143
- Schechter, P. L., Gregg, M. D., Becker, R. H., Helfand, D. J., & White, R. L. 1998, AJ, 115, 1371
- Schneider, D. P., et al. 2007, AJ, 134, in press
- Schneider, D. P., et al. 2005, AJ, 130, 367
- Sluse, D., Surdej, J., Claeskens, J.-F., Hutsemékers, D., Jean, C., Courbin, F., Nakos, T., Billeres, M., & Khmil, S. V. 2003, A&A, 406, L43
- Smith, A., et al. 2002, AJ, 123, 2121
- Spergel, D. N., et al. 2003, ApJS, 148, 175
- Stoughton, C., et al. 2002, AJ, 123, 485
- Surdej, J., Swings, J.-P., Magain, P., Courvoisier, T. J.-L., & Borgeest, U. 1987, Nature, 329, 695
- Tucker, D. L., et al. 2006, AN, 327, 821
- Walsh, D., Carswell, R. F., & Weymann, R. J. 1979, Nature, 279, 381
- Weymann, R. J., et al. 1980, Nature, 285, 641
- Williams, K. A., Momcheva, I., Keeton, C. R., Zabludoff, A. I., Lehár, J. 2006 ApJ, 646, 85
- York, D. G., et al. 2000, AJ, 120, 1579

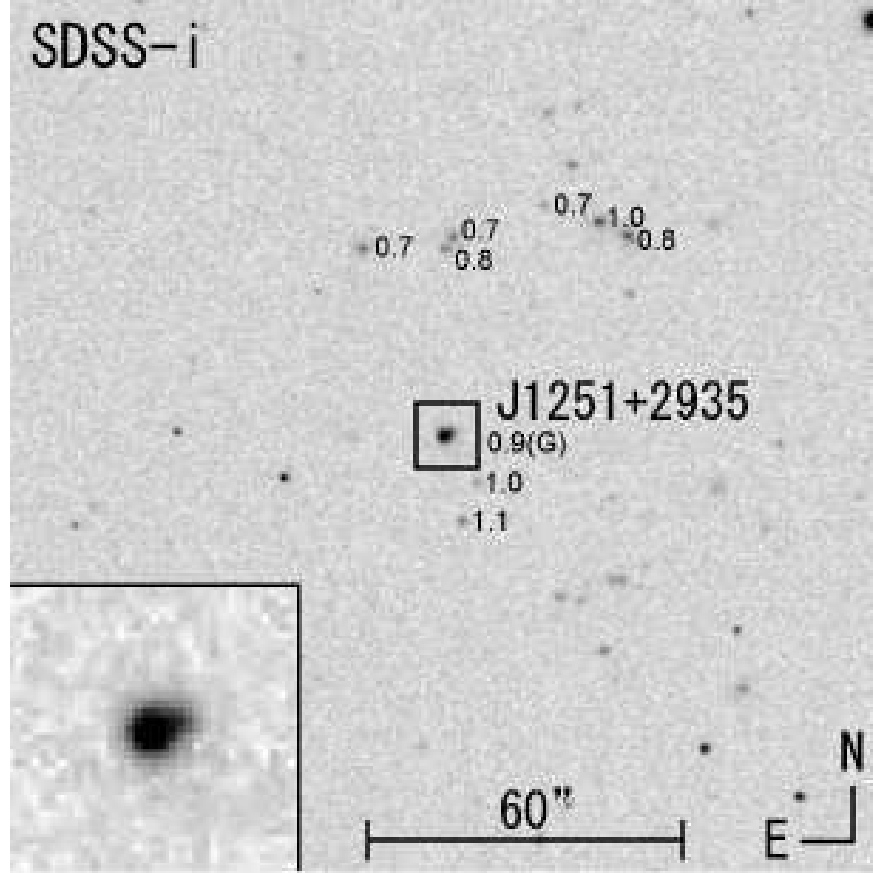


Fig. 1.— SDSS *i*-band image of the SDSS J1251+2935 field ($1''.2$ seeing, 54 sec exposure). The pixel scale is $0''.396 \text{ pixel}^{-1}$, North is up and East is left. An expanded view of SDSS J1251+2935 is shown in the inset at lower left. Small numbers beside galaxies are $R - I$ colors from the Optic images.

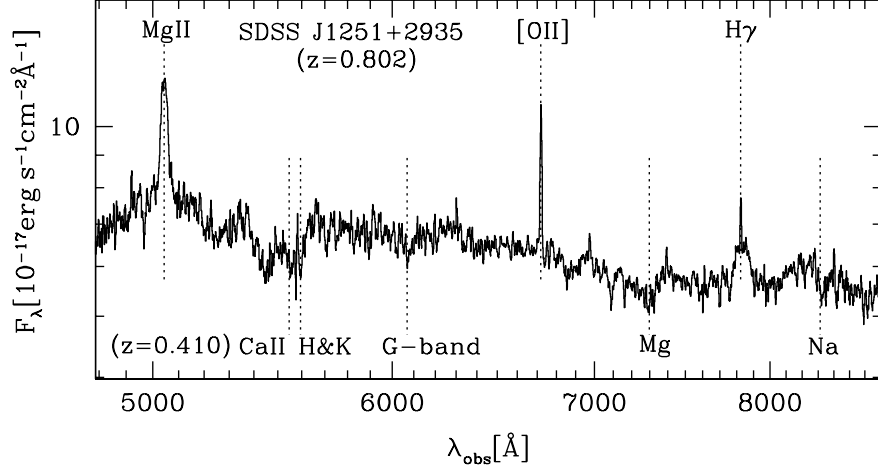


Fig. 2.— SDSS spectrum of SDSS J1251+2935 with a resolution of ~ 1800 . The quasar emission lines (Mg II, [O II], and H γ) redshifted to $z = 0.802$ are marked by the dashed lines and the galaxy absorption lines (Ca H&K, G-band, Mg, and Na) redshifted to $z = 0.410$ are marked by the dotted lines. The galaxy absorption lines indicate the existence of a bright lensing galaxy.

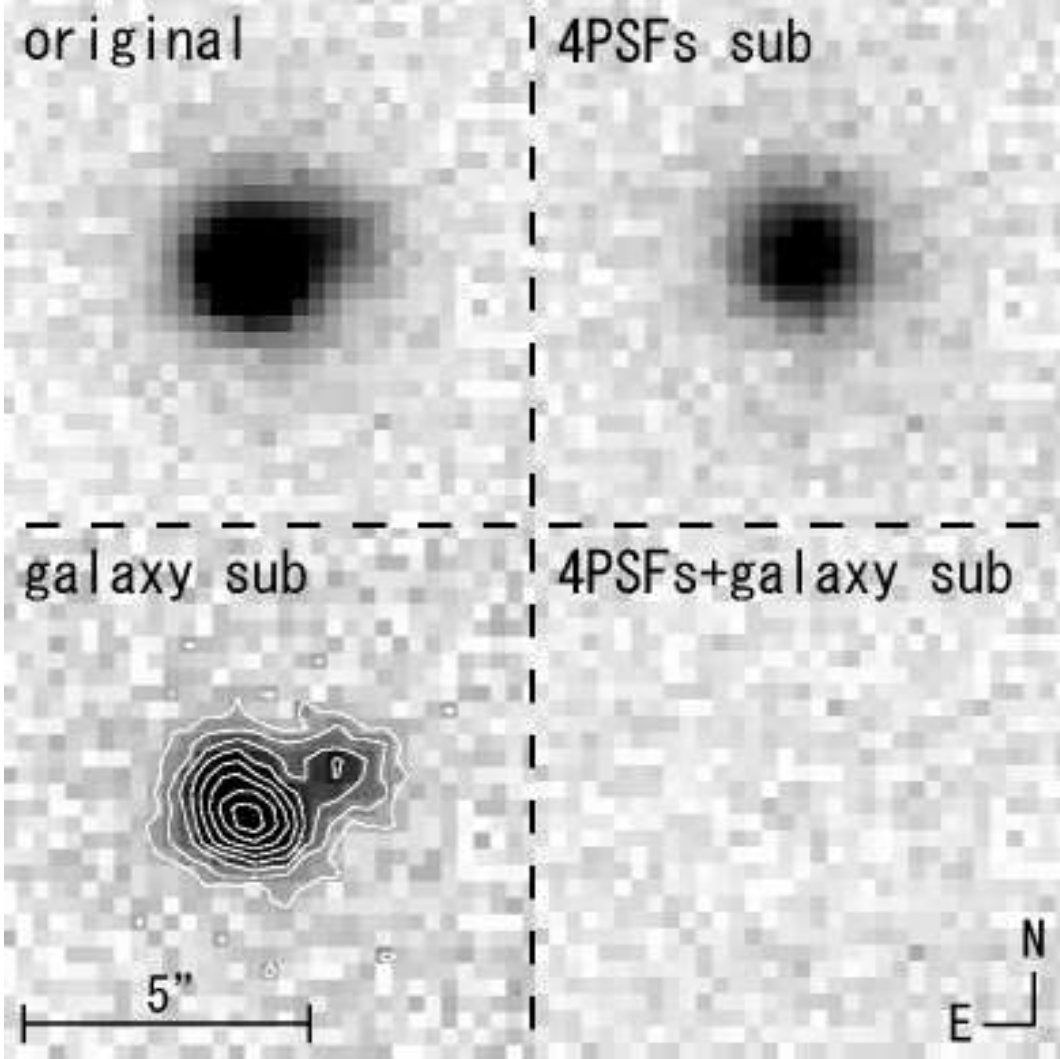


Fig. 3.— Optic *I*-band image of SDSS J1251+2935. The upper-left panel is the original data. The galaxy-like extended object in the upper-right panel is the residual after subtracting only 4 point-like components, and vice versa in the lower-left (overplotted with contours). There are no residuals after subtracting a galaxy and 4 PSFs, as shown in the lower-right panel. The images and contours are scaled by the square-root of the counts.

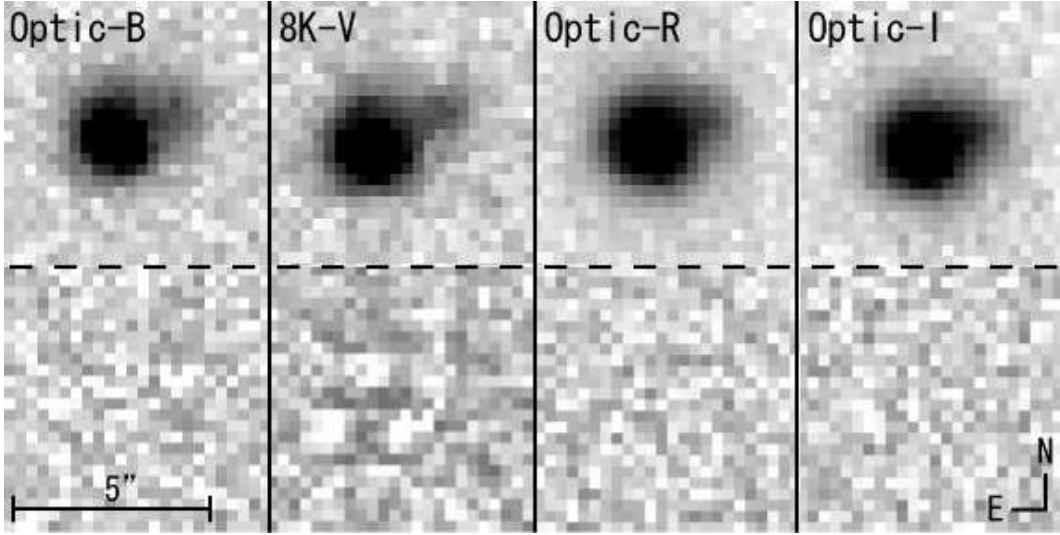


Fig. 4.— Original Optic (BRI) and UH8k (V) images of SDSS J1251+2935 (upper panels) and the residuals after subtracting the best models (lower panels). The best models consist of 4 PSFs for the Optic B -band and UH8k V -band, and 4 PSFs plus a galaxy for Optic R and I -bands. The pixel scales of Optic and UH8k are $0''.274 \text{ pixel}^{-1}$ (2×2 binned) and $0''.232 \text{ pixel}^{-1}$, respectively. Although there are some residuals in the V -band image due to the galaxy, its flux is too small to be measured accurately.

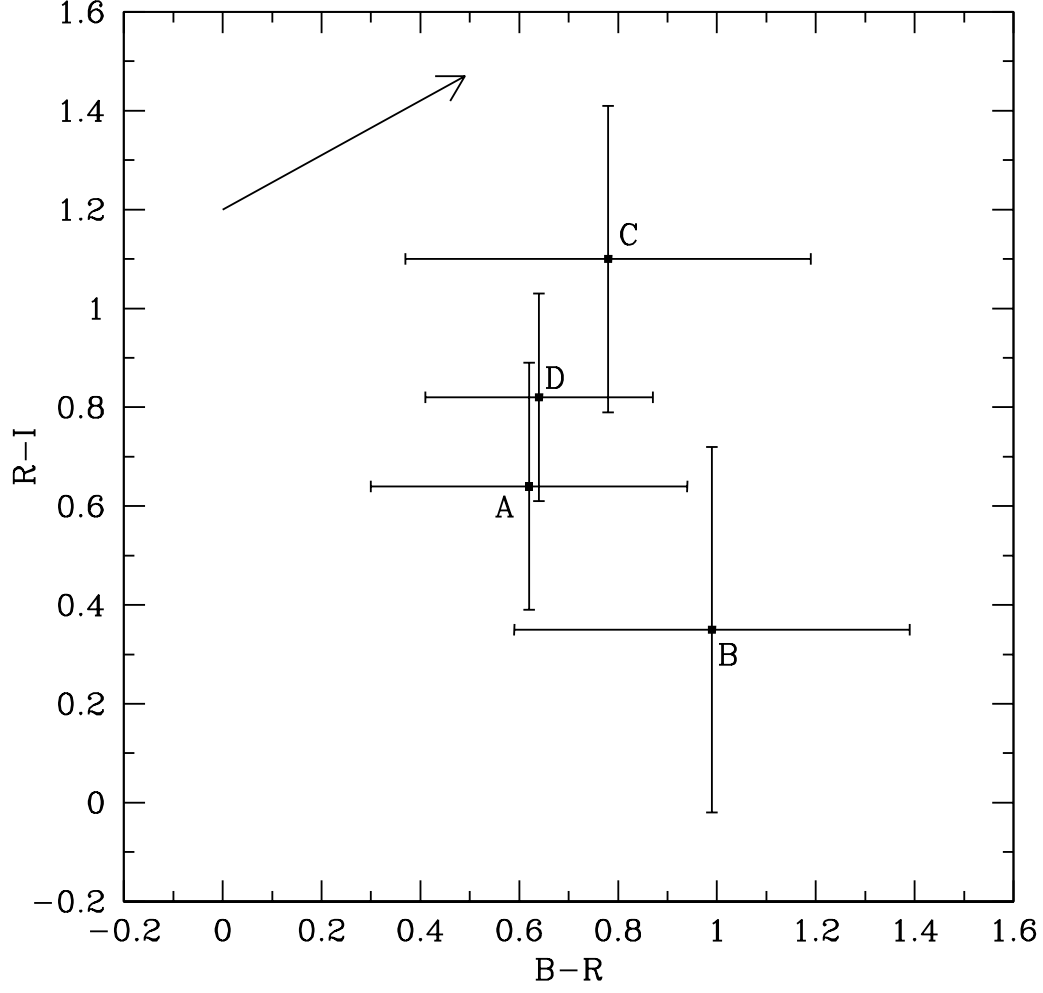


Fig. 5.— Color-color diagram ($B-R$ and $R-I$) of the 4 point-like components. The arrow upper-left indicates the extinction direction for a Cardelli et al. (1989) extinction law with $R_V = 3.1$ and $\Delta(B-V) = 0.3$.

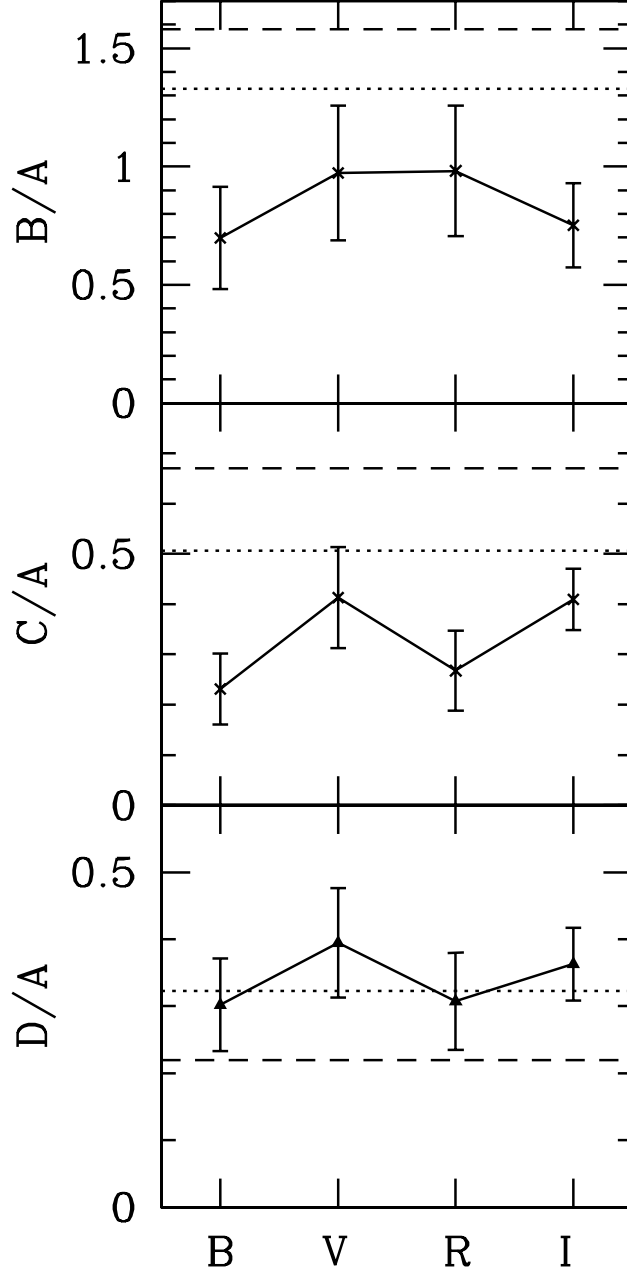


Fig. 6.— Flux ratios of the 4 point-like components. The flux ratios predicted by the SIE model (without flux ratio constraints) and the SIE plus external shear model (with the R -band flux ratio constraints and the weak constraints on the ellipticity and the position angle of the lens galaxy) in §4 are plotted as *dashed* and *dotted* lines, respectively. Note that the latter model fits the observation with $\chi^2_{\text{red}} = 2.5$.

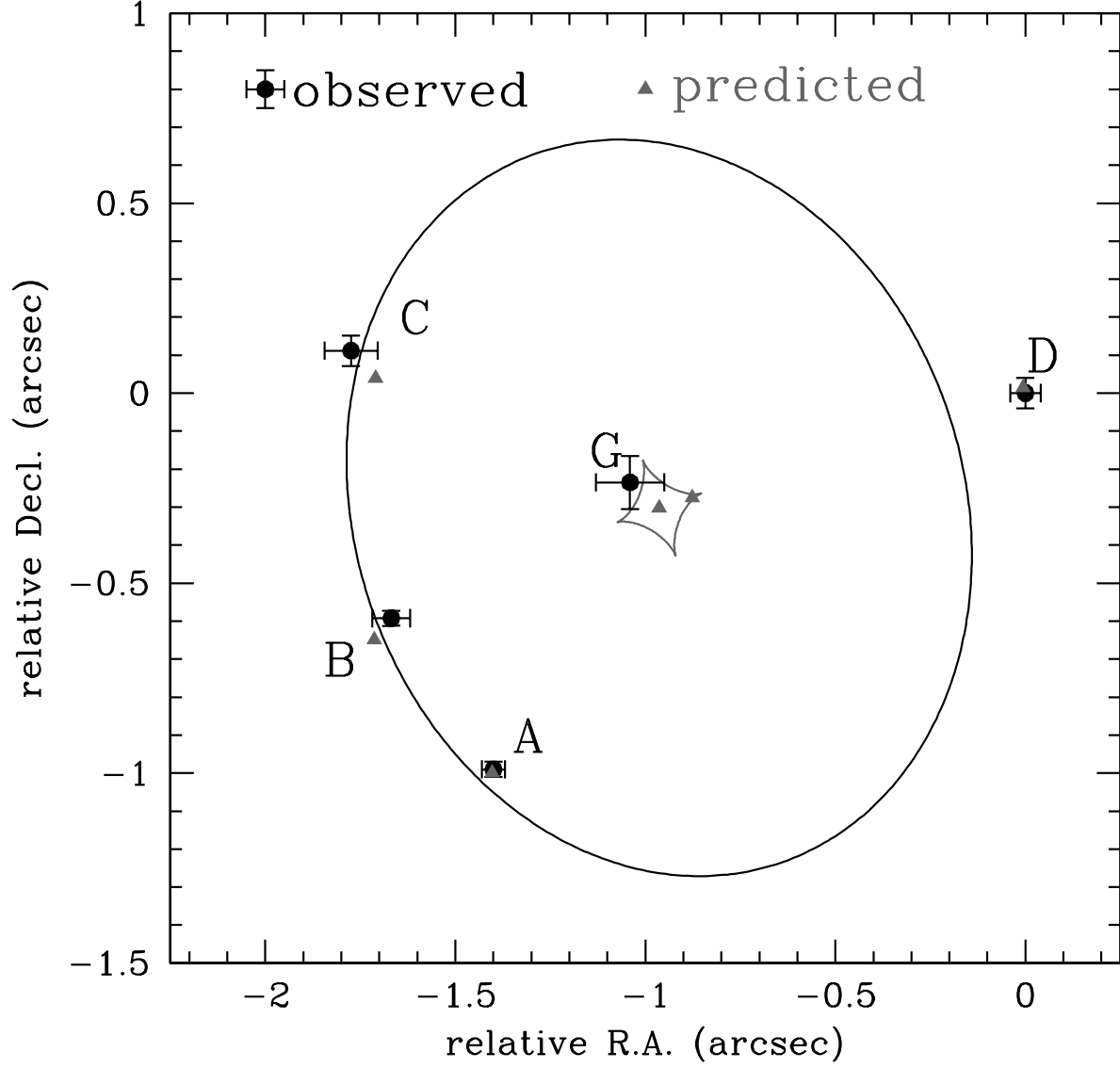


Fig. 7.— Predicted and observed positions of components A–D and G. The filled circles with error bars represents the observed positions, and the gray filled triangles represent the positions predicted by the SIE model. The critical curve (*black line*) and the caustics (*gray line*) are also plotted. The gray filled triangle on the caustics is the predicted source plane position of the quasar.

Table 1. ASTROMETRY AND PHOTOMETRY OF SDSS J1251+2935

Object	$x[\text{arcsec}]^{\text{a}}$	$y[\text{arcsec}]^{\text{a}}$	B^{b}	R^{b}	I^{b}
A	-1.40 ± 0.03	-1.00 ± 0.02	20.67 ± 0.22	20.05 ± 0.23	19.41 ± 0.10
B	-1.67 ± 0.05	-0.65 ± 0.02	21.06 ± 0.31	20.07 ± 0.25	19.72 ± 0.27
C	-1.77 ± 0.07	0.04 ± 0.04	22.26 ± 0.30	21.48 ± 0.28	20.38 ± 0.14
D	0.00 ± 0.04	0.00 ± 0.04	21.97 ± 0.16	21.33 ± 0.16	20.51 ± 0.14
G	-1.04 ± 0.09	-0.23 ± 0.07	\dots	19.32 ± 0.16	18.43 ± 0.25

^aMeasured in the Optic R -band image using GALFIT. The positive directions of x and y are West and North, respectively. Errors indicate the dispersions from 6 different PSF templates.

^bMeasured in the Optic images using GALFIT. The errors are the dispersions from 6 different PSF templates, and they do not include the absolute calibration uncertainties. The magnitudes are calibrated using the standard star PG0918+029 (Landolt 1992).

Table 2. SDSS J1251+2935: MASS MODELS

Model	Data ^a	$\chi^2_{\text{tot}}/\text{dof}^{\text{b}}$	$\chi^2_{\text{flux}}^{\text{c}}$	$R_{\text{E}}[\text{arcsec}]$	e	$\theta_e[\text{deg}]$	γ	$\theta_\gamma[\text{deg}]$	comments
SIE	pos	3.3/3	(20)	0.88	0.19	19	bad flux
SIE+shear	pos	0.062/1	(18)	0.79	0.66	10	0.21	−80	large misalignment
SIE+shear	pos+shape	3.7/3	(16)	0.87	0.21	25	0.018	−8.7	bad flux
SIE	pos+flux	17/6	8.8	0.80	0.46	18	poor fitting
SIE+shear	pos+flux	8.9/4	1.1	0.76	0.67	53	0.28	−32	large misalignment
SIE+shear	pos+flux+shape	15/6	6.3	0.83	0.38	34	0.074	−15	poor fitting

Note. — Results of various mass models constrained by R -band data. The position angles are measured East of North. The time delay between images A and D in the SIE model is $\Delta t_{AD} \sim 17 h^{-1}\text{day}$.

^aData used to constrain the models; pos: positions of the 4 images and the galaxy, flux: fluxes of the 4 images, and shape: weak constraints on the ellipticity and position angle of the lens galaxy ($e = 0.28 \pm 0.15$ and $\theta = 26^\circ \pm 10^\circ$).

^bTotal χ^2 and the degree of freedom.

^cContribution of fluxes to the χ^2 . The values in parentheses are not included in χ^2_{tot} .